



CONCRETE FRACTURE ANALYSIS USING THE CONTINUUM STRONG DISCONTINUITY APPROACH AND THE BOUNDARY ELEMENT METHOD

Rodrigo G. Peixoto

Gabriel O. Ribeiro

Roque L. S. Pitangueira

rodrigo.peixoto@dees.ufmg.br

gabriel@dees.ufmg.br

roque@dees.ufmg.br

Dep. de Eng. de Estruturas, Escola de Engenharia, Universidade Federal de Minas Gerais

Avenida Antônio Carlos, 6627, CEP: 31270-901, Belo Horizonte, Minas Gerais, Brazil

Abstract. *The implicit formulation of the boundary element method is applied to bi-dimensional problems of material failure involving, sequentially, inelastic dissipation with softening in continuous media, bifurcation and transition between weak and strong discontinuities. The bifurcation condition is defined by the singularity of the localization tensor, also known, for historical reasons, as acoustic tensor. The weak discontinuities are related to strain localization bands of finite width, which become increasingly narrow until to collapse in a surface with discontinuous displacement field, called strong discontinuity surface. To associate such steps to the fracture process in concrete specimens, an isotropic damage (continuum) constitutive model is used to represent the material behaviour in all of them, taking into account the adaptations that come from the strong discontinuity analysis for the post-bifurcation phases. The crack propagation across the domain is done by an automatic cells generation algorithm and, in this context, the fracture process zone in the crack tip became totally represented by the cells in the continuum damage regime and the cells with weak discontinuities.*

Keywords: *Concrete fracture, Damage constitutive models, Continuum Strong Discontinuity Approach, Boundary Element Method*

1 INTRODUCTION

The first developments of boundary integral equations for the treatment of non-linear material behaviour may be attributed to Swedlow and Cruse (1971), Mendelson (1973), Riccardella (1973) and Mukherjee (1977). Later, Bui (1978) presented a corrected way to evaluate derivatives of the singular integrals involving the inelastic fields, introducing new free terms. Those results were then applied to the Boundary Element Method (BEM) by Telles and Brebbia (1979). They used an explicit formulation, where the increment of the initial fields explicitly appears in the non-linear discretized equations and the equilibrium is achieved by a recursive procedure. Considering the proportional relationship between rates of stress and elastic strain, Telles and Carrer (1991) proposed an implicit formulation, where the initial field increments are written in terms of total strain, resulting in an equilibrium matrix equation, which is linearised and incrementally solved. In all above references, elastoplastic constitutive models were considered.

Some material behaviour, e.g., the quasi-brittle ones, requires the introduction of strain softening laws for a correct representation. A direct way to do this is to consider a plasticity model with yield limit degradation, as done by Lin et al. (2002) and Sládek et al. (2003). The presence of strain softening results in a loss of objectiveness with respect to mesh refinements, as the solution tends to an infinitely small localization bandwidth with zero energy dissipation during failure. For that reason, in both works, a non-local procedure, based on the spatial averaging of the plastic multiplier, was also introduced. They differ mainly by the boundary stress evaluation: in the first work, constant functions are used to approximate initial fields inside cells, while, in the second, a regularization of the hypersingular integral equation is adopted. Another non-local plasticity model, based on a re-definition of the yield surface, including a dependency on the Laplacian of the plastic multiplier, was applied to the implicit formulation by Benallal et al. (2002). In that work, a complementary integral representation of the plastic multiplier was discretized and solved together (in a coupled way) to the incremental implicit equation.

An alternative (and perhaps more elegant) way to deal with material's loss of strength, is the adoption of constitutive models based on continuum damage mechanics (CDM). In the BEM context, some works can be cited, such as Rajgelj et al. (1992), Herding and Kuhn (1996), García et al. (1999) and Botta et al. (2005). As expected, they also reported mesh dependence when this model is locally applied and an averaging procedure of some strain invariants was introduced, regularizing the model. A more detailed discussion on such localization problems is made by the same authors in a subsequent paper (Benallal et al., 2006).

The Continuum Strong Discontinuity Approach (CSDA), originally introduced by Simo et al. (1993) and later deepened by Oliver (1996), is based on the introduction of discontinuous jumps in the displacement field, which results in unbounded strain values at these points. A continuum constitutive model, equipped with an appropriate softening law, is then applied to characterize the dissipation effects on the discontinuity surface. From the continuity condition of the traction vector across this discontinuity surface, additional equations arrive and are used to evaluate the current displacement jump components. Also, the bounded character of the stress tensor (from its physical sense) leads to a re-interpretation of the hardening-softening modulus of the continuum constitutive model, where the Dirac's delta distribution, associated to an infinitesimally small strain localization band, appears in the new expression. An analysis of the total amount of energy spent for the discontinuity formation, complements such expres-

sion introducing, beyond other parameters, the material's fracture energy. This methodology overcomes the mesh dependence associated to strain localization and was applied to the implicit formulation of the BEM by Manzoli and Venturini (2004, 2007), Manzoli et al. (2009) and Peixoto et al. (2015). A common feature of these works is the direct introduction of a discontinuity surface when the elastic limit is reached. The orientation of such surface is taken as perpendicular to the direction of the first principal stress.

In this work, a more rigorous criterion is assumed to define the onset and the direction of a discontinuity surface: the (material) bifurcation analysis based on the singularity of the localization tensor. Also, if the so called discontinuity conditions are not achieved on the bifurcation time, a weak discontinuity phase (in which discontinuities are present in the strain fields with the displacements remaining constants) precludes the strong discontinuity situation. An appropriate isotropic damage constitutive model for concrete behaviour representation is adopted. In this way, it is possible to identify three regions that form the called fracture process zone (FPZ): a diffuse zone, where dissipation occurs in continuous media; a weak discontinuity zone, representing the strain localization inside bands with increasingly narrow widths, physically associated to presence of micro-cracks; and a strong discontinuity zone, with discontinuous displacements, representing macro-cracks. Such process is illustrated in Fig. 1.

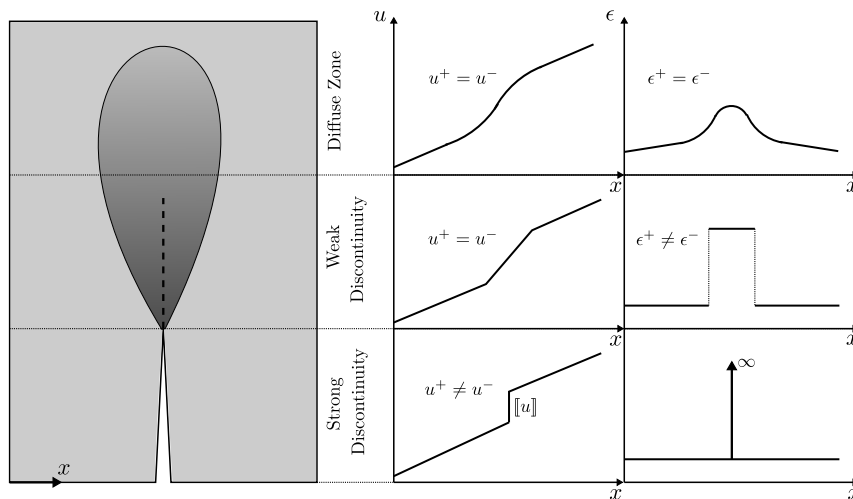


Figure 1: Representation of FPZ, u : displacement, ϵ : strain

An automatic cell generation algorithm was implemented to track the crack propagation over the solid and two concrete fracture examples are presented to demonstrate the accuracy of the methodology.

2 STRAIN LOCALIZATION IN A DAMAGE CONSTITUTIVE MODEL

Strain localization, characterized by high displacement gradients in narrow bands, may be understood as a material instability associated mainly to the presence of softening in the macroscopic constitutive modelling. Such bands are generally delimited by strain discontinuity surfaces (*weak discontinuities*) and its onset is determined by the material bifurcation analysis. This process is described here in the light of a specific isotropic damage constitutive model.

2.1 Isotropic damage constitutive model

To represent the behaviour of quasi-brittle materials, such as concrete, an isotropic damage constitutive model, in which damage evolution occurs preferentially under traction states, was chosen. This model is the same used in Oliver et al. (2006) and can be briefly stated by the next expressions:

$$\text{Free energy: } \psi(\epsilon_{ij}, r) = [1 - D(r)]\psi_o(\epsilon_{ij}), \quad \psi_o(\epsilon_{ij}) = \frac{1}{2}\epsilon_{ij}E_{ijkl}^o\epsilon_{kl}; \quad (1a)$$

$$\text{Constitutive equation: } \sigma_{ij} = \frac{\partial\psi(\epsilon_{ij}, r)}{\partial\epsilon_{ij}} = (1 - D)E_{ijkl}^o\epsilon_{kl} = E_{ijkl}\epsilon_{kl}; \quad (1b)$$

$$\text{Damage variable: } D \equiv D(r) = 1 - \frac{q(r)}{r}, \quad D \in [0, 1]; \quad (1c)$$

$$\text{Internal variable evolution law: } \dot{r} = \dot{\lambda}, \quad \begin{cases} r \in [r_o, \infty), \\ r_o = r|_{t=0} = \frac{f_t}{\sqrt{E}}; \end{cases} \quad (1d)$$

$$\text{Damage criterion: } \begin{cases} F(\sigma_{ij}, q) \equiv \tau_\sigma - q = \sqrt{\sigma_{ij}^+ E_{ijkl}^{o,-1} \sigma_{kl}} - q \quad (\text{stress space}) \\ \text{or} \\ \bar{F}(\epsilon_{ij}, r) \equiv \tau_\epsilon - r = \sqrt{\epsilon_{ij}^+ E_{ijkl}^o \epsilon_{kl}} - r \quad (\text{strain space}); \end{cases} \quad (1e)$$

$$\text{Loading-unloading conditions: } F \leq 0, \quad \dot{\lambda} \geq 0, \quad \dot{\lambda}F = 0, \quad \dot{\lambda}\dot{F} = 0 \quad (1f)$$

$$\text{Hardening rule: } \dot{q} = H(r)\dot{r}, \quad (H = q'(r) \leq 0), \quad \begin{cases} q \in [0, r_o], \\ q|_{t=0} = r_o \end{cases} \quad (1g)$$

where ϵ_{ij} is the linear strain tensor given by $\epsilon_{ij} = \frac{1}{2}(u_{i,j} + u_{j,i})$, with u_i representing the displacement field, σ_{ij} , E_{ijkl}^o and $E_{ijkl} = (1 - D)E_{ijkl}^o$ are, respectively, the Cauchy's stress tensor, the linear elastic isotropic constitutive tensor and the secant constitutive tensor, q is the stress-like internal variable, while r is the strain-like internal variable. The value r_o is the threshold that determines the initial elastic domain, which can be characterized in terms of the uniaxial elastic strength f_t and the elastic modulus E - see Eq. (1d). The parameter H is called as hardening-softening modulus. In Eq. (1e), the norms τ_σ and τ_ϵ are correspondent in a constitutive point of view and, particularly the second one, is usually known as equivalent strain. Moreover, the tensor ϵ_{ij}^+ is defined (in a coordinates system aligned with the principal strain directions) by:

$$\epsilon_{ij}^+ = \sum_{k=1}^{n_{dim}} \langle \epsilon_k \rangle \hat{\mathbf{e}}_k \otimes \hat{\mathbf{e}}_k \quad (2)$$

where ϵ_k represents the k -th principal strain, $\hat{\mathbf{e}}_k$ is the unit vector in the corresponding principal direction and $\langle \epsilon_k \rangle = (|\epsilon_k| + \epsilon_k)/2$. Also, $\sigma_{ij}^+ := (1 - D)E_{ijkl}^o\epsilon_{kl}^+$.

From Eqs. (1b), (1c), (1e) and (1f), a tangent constitutive relation can be written as

$$\dot{\sigma}_{ij} = E_{ijkl}^t \dot{\epsilon}_{kl}; \quad E_{ijkl}^t = E_{ijkl} - \left(\frac{\partial D}{\partial r} \right) \left(\frac{\partial \tau_\epsilon}{\partial \epsilon_{kl}} \right) E_{ijrs}^o \epsilon_{rs} \quad (3)$$

where E_{ijkl}^t is called as the constitutive tangent tensor (or operator).

2.2 Material bifurcation analysis

The moment of the inelastic loading when the strain localization phenomenon begins is known as discontinuous (material) bifurcation time. As the name suggests, after that moment, the dissipation process continues only inside the localization band whereas elastic unloading (or neutral loading) takes place outside. A necessary condition to it happen is that the localization tensor, $Q_{jk} := n_i E_{ijkl}^t n_l$, becomes singular (van der Giessen and de Borst, 1998), i.e.,

$$\det(Q_{jk}) = \det(n_i E_{ijkl}^t n_l) = 0 \quad (4)$$

where n_i is the unitary vector normal to the bandwidth orientation, as illustrated in Fig. 2.

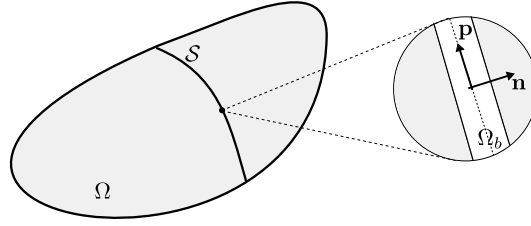


Figure 2: Solid body with a strain localization band Ω_b

Strictly speaking, Eq. (4) refers to a condition for continuous bifurcation, in which the tangent constitutive operators inside and outside the band are the same. However, Rice and Rudnicki (1980) shown that such condition corresponds to a limit case of discontinuous bifurcation with tendency to first occur during the inelastic loading.

The substitution of Eq. (3) in Eq. (4) results, usually, in a optimization problem of find, between all possible directions that satisfies the singularity condition (if exists at least one), the n_i that gives the maximum softening modulus, H . However, considering the constitutive model presented in Sec. 2.1, closed forms for a critical softening modulus, H^{crit} , and the associated band orientation can be obtained for plane problems, as detailed in Peixoto (2016). Such expressions are summarized in the following:

$$H^{crit}(\theta) = \frac{q}{r} \left[1 - \frac{r^2}{r^2 - \gamma \epsilon_{pp}(\theta) \epsilon_{pp}^+(\theta)} \right]; \quad \gamma = \begin{cases} E & \text{for plane stress} \\ \frac{E}{1 - \nu^2} & \text{for plane strain} \end{cases} \quad (5)$$

$$\epsilon_{pp}(\theta) = (\epsilon_1 - \epsilon_2) \sin^2 \theta + \epsilon_2, \quad \epsilon_{pp}^+(\theta) = (\langle \epsilon_1 \rangle - \langle \epsilon_2 \rangle) \sin^2 \theta + \langle \epsilon_2 \rangle \quad (6)$$

$$\sin^2 \theta = \mathcal{G}(\epsilon_1, \epsilon_2) = - \left[\frac{\epsilon_2 (\langle \epsilon_1 \rangle - \langle \epsilon_2 \rangle) + \langle \epsilon_2 \rangle (\epsilon_1 - \epsilon_2)}{2(\epsilon_1 - \epsilon_2) (\langle \epsilon_1 \rangle - \langle \epsilon_2 \rangle)} \right] \quad (7)$$

$$\sin^2 \theta^{crit} = \begin{cases} \mathcal{G}(\epsilon_1, \epsilon_2) & \text{if } 0 \leq \mathcal{G}(\epsilon_1, \epsilon_2) \leq 1 \\ 1 & \text{if } \mathcal{G}(\epsilon_1, \epsilon_2) > 1 \\ 0 & \text{if } \mathcal{G}(\epsilon_1, \epsilon_2) < 0 \end{cases} \quad (8)$$

where ν is the Poisson ratio, ϵ_{pp} is the strain component in the \mathbf{p} direction indicated in Fig. 2, θ is the angle between the first principal direction and \mathbf{n} , and θ^{crit} is the orientation of the localization band associated to H^{crit} .

3 WEAK AND STRONG DISCONTINUITIES

In the above section, the necessary conditions to initiate the strain localization phenomenon was pointed out. Here, the subsequent steps are treated, i.e., the transition from weak to strong discontinuities, which can be interpreted as a variable bandwidth model.

3.1 Kinematics

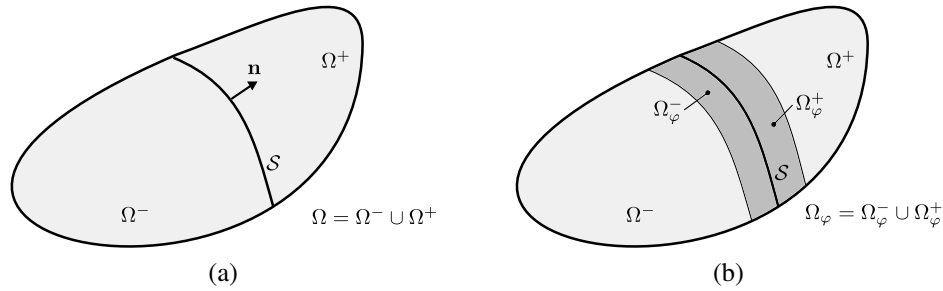


Figure 3: Solid with discontinuity surface

Referring to Fig. 3a, the rate of displacement vector field can be written as

$$\dot{u}_i(\mathbf{X}, t) = \bar{\dot{u}}_i(\mathbf{X}, t) + \mathcal{H}_S(\mathbf{X})[[\dot{u}_i]](\mathbf{X}, t) \quad (9)$$

where $\bar{u}_i(\mathbf{X}, t)$ is the regular part of the displacement field and $[[u_i]](\mathbf{X}, t)$ are continuous functions over the solid domain that represent the displacement jump in the discontinuity surface \mathcal{S} , supported by the Heaviside function $\mathcal{H}_S(\mathbf{X})$ ($\mathcal{H}_S = 1 \forall \mathbf{X} \in \Omega^+$ and $\mathcal{H}_S = 0 \forall \mathbf{X} \in \Omega^-$).

Now, lets assume the following (rate of) strain field:

$$\begin{aligned} \dot{\epsilon}_{ij}(\mathbf{X}, t) &= \underbrace{\frac{1}{2}(\bar{\dot{u}}_{i,j} + \bar{\dot{u}}_{j,i}) + \frac{\mathcal{H}_S}{2}([[\dot{u}_{i,j}]] + [[\dot{u}_{j,i}]])}_{\bar{\dot{\epsilon}}_{ij}} + \frac{\mu_S}{2h} ([[\dot{u}_i]] n_j + [[\dot{u}_j]] n_i) \\ &= \bar{\dot{\epsilon}}_{ij} + \frac{\mu_S}{2h} ([[\dot{u}_i]] n_j + [[\dot{u}_j]] n_i) \end{aligned} \quad (10)$$

where $\bar{\epsilon}_{ij}$ is the regular part of the strain field exhibiting, at most, bounded discontinuities across \mathcal{S} , μ_S is a collocation function over \mathcal{S} , i.e., $\{\mu_S(\mathbf{X}) = 1 \text{ if } \mathbf{X} \in \mathcal{S} \text{ and } \mu_S(\mathbf{X}) = 0 \text{ if } \mathbf{X} \notin \mathcal{S}\}$ and h is a kinematic regularization parameter, such that

$$\left\{ \begin{array}{l} \text{Weak discontinuity regime: } h \neq 0 \\ \text{Strong discontinuity regime: } h \rightarrow 0 \Rightarrow \left(\frac{\mu_S}{h} \right) \rightarrow \delta_S \end{array} \right. \quad (11)$$

where δ_S is the Dirac's line delta-function over \mathcal{S} .

Thus, the kinematic Eq. (10) may be used indistinguishably to represent the weak and strong regimes. However, it is important to note that compatibility with Eq. (9) is achieved only in the second case. Moreover, Eq. (10) can be integrated until an instant of time in the strong

discontinuity regime, i.e., $t \geq t_{SD}$, resulting in:

$$\begin{aligned} \epsilon_{ij}(\mathbf{X}, t)|_{t \geq t_{SD}} &= \underbrace{\int_0^t \dot{\epsilon}_{ij} dt + \frac{\mu_S}{2} \int_{t_B}^{t_{SD}} \frac{1}{h} (\llbracket \dot{u}_i \rrbracket n_j + \llbracket \dot{u}_j \rrbracket n_i) dt}_{\bar{\epsilon}_{ij}} + \frac{\mu_S}{2} \int_{t_{SD}}^t \frac{1}{h} (\llbracket \dot{u}_i \rrbracket n_j + \llbracket \dot{u}_j \rrbracket n_i) dt \\ &= \bar{\epsilon}_{ij} + \mu_S \frac{1}{2h} (\Delta \llbracket u_i \rrbracket n_j + \Delta \llbracket u_j \rrbracket n_i) \end{aligned} \quad (12)$$

where $\Delta \llbracket u_i \rrbracket = \llbracket u_i \rrbracket(\mathbf{X}, t) - \llbracket u_i \rrbracket(\mathbf{X}, t_{SD})$ is the displacement jump increment during the strong discontinuity regime and the material character for the discontinuity surface, i.e., $\dot{n}_i = 0$, was adopted.

As detailed by Oliver (1996), the imposition of essential boundary conditions cannot be done just on one of the fields \bar{u}_i or $\llbracket u_i \rrbracket$, and a reformulation of the kinematics needs to be performed. Such reformulation begins with the assumption of an additional arbitrary sub-domain $\Omega_\varphi \subset \Omega$ surrounding \mathcal{S} as presented in Fig. 3b. It is assumed that the boundary Γ_u , where the essential boundary conditions are imposed, is outside Ω_φ ($\Gamma_u \cap \Omega_\varphi = \emptyset$).

Then, one can define a continuous function $\varphi(\mathbf{X})$ which is completely arbitrary except for the following two conditions:

$$\begin{aligned} \varphi(\mathbf{X}) &= 0, \forall \mathbf{X} \in \Omega^- \setminus \Omega_\varphi^- \\ \varphi(\mathbf{X}) &= 1, \forall \mathbf{X} \in \Omega^+ \setminus \Omega_\varphi^+ \end{aligned} \quad (13)$$

where $a \setminus b$ means a excluding b .

Equation (9) can now be rewritten as

$$\begin{aligned} \dot{u}_i(\mathbf{X}, t) &= \underbrace{\dot{\hat{u}}_i(\mathbf{X}, t) + \varphi(\mathbf{X}) \llbracket \dot{u}_i \rrbracket(\mathbf{X}, t)}_{\hat{u}_i(\mathbf{X}, t)} + \underbrace{[\mathcal{H}_\mathcal{S}(\mathbf{X}) - \varphi(\mathbf{X})] \llbracket \dot{u}_i \rrbracket(\mathbf{X}, t)}_{\mathcal{M}_\mathcal{S}^h(\mathbf{X})} \\ &= \hat{u}_i(\mathbf{X}, t) + \mathcal{M}_\mathcal{S}^h(\mathbf{X}) \llbracket \dot{u}_i \rrbracket(\mathbf{X}, t) \end{aligned} \quad (14)$$

where $\hat{u}_i(\mathbf{X}, t)$ are continuous functions and $\mathcal{M}_\mathcal{S}^h(\mathbf{X})$ takes zero value everywhere in Ω , except in Ω_h .

Hence, the kinematic description of the displacement field is made now, according to Eq. (14), in terms of the regular part $\hat{u}(\mathbf{X}, t)$ plus the term $\mathcal{M}_\mathcal{S}^h(\mathbf{X}) \llbracket u_i \rrbracket(\mathbf{X}, t)$, which contains the jump and whose support is Ω_φ . Thus, the essential boundary conditions can be applied exclusively on the term $\hat{u}(\mathbf{X}, t)$.

In an analogous way, Eq. (10) assumes the form

$$\begin{aligned} \dot{\epsilon}_{ij} &= \frac{1}{2} (\dot{\hat{u}}_{i,j} + \dot{\hat{u}}_{j,i}) + \underbrace{\frac{\mathcal{M}_\mathcal{S}^h}{2} (\llbracket \dot{u}_{i,j} \rrbracket + \llbracket \dot{u}_{j,i} \rrbracket) - \frac{1}{2} (\varphi_{,i} \llbracket \dot{u}_j \rrbracket + \varphi_{,j} \llbracket \dot{u}_i \rrbracket)}_{-\dot{\epsilon}_{ij}^\varphi} + \frac{\mu_S}{2h} (\llbracket \dot{u}_i \rrbracket n_j + \llbracket \dot{u}_j \rrbracket n_i) \\ &= \dot{\hat{\epsilon}}_{ij} - \dot{\epsilon}_{ij}^\varphi + \frac{\mu_S}{2h} (\llbracket \dot{u}_i \rrbracket n_j + \llbracket \dot{u}_j \rrbracket n_i) \end{aligned} \quad (15)$$

where $\dot{\hat{\epsilon}}_{ij}$ is a regular part, $\dot{\epsilon}_{ij}^\varphi$ have non-zero values only inside the sub-domain Ω_φ and the last term is limited to the discontinuity line \mathcal{S} .

3.2 Strong discontinuity analysis

In the CSDA, continuous constitutive models (e.g., the isotropic damage model presented in Sec. 2.1) are used to describe the dissipation phenomena over a discontinuity interface. For that reason, the main issue that arises is the identification of the conditions that make the strong discontinuity kinematics, described above, compatible with such continuum constitutive modelling. This analysis, commonly called Strong Discontinuity Analysis (SDA), is detailed in Oliver (2000) and shows as a result that is possible to write a discrete (or cohesive) constitutive model, that relates traction to displacement jumps instead stress to strain, associated to the continuum one.

Some theoretical remarks of the SDA are presented in this section. First, from the discontinuity interface equilibrium condition, a non-linear equation for the displacement jump evaluation is obtained. Then, a regularized constitutive equation, which can be considered inside BEM cells domains, from the solution of this equation, is established. Finally, a re-interpretation of the hardening-softening modulus of the continuous constitutive model, based on the bounded character of the stress tensor either in points with unbounded strain over the discontinuity interface, is presented.

Discontinuity interface equilibrium

As mentioned earlier, an appropriate continuum constitutive model is used to describe the dissipation process on points over the discontinuity line \mathcal{S} . The constitutive equation, relating stress to the total strain, of a such model is generically represented here by

$$\dot{\sigma}_{ij}^{\mathcal{S}}(\dot{\epsilon}_{ij}) \equiv \dot{\sigma}_{ij}^{\mathcal{S}}(\dot{\hat{\epsilon}}_{ij}, \llbracket \dot{u}_i \rrbracket, \llbracket \dot{u}_{i,j} \rrbracket) \quad (16)$$

where $\dot{\epsilon}_{ij}$ is given by Eq. (15) and the dependence on $\varphi(\mathbf{X})$ and n_i were avoided by the arbitrariness of the first and by considering the material character of the discontinuity, i.e., once initiated, its orientation remains fixed. Also, the dependence on h is overcome by the introduction of a pre-defined bandwidth evolution law, as described further on.

Domain points outside of \mathcal{S} are considered in this work to stay in a linear elastic regime. Thus, the constitutive relation for these points can be written as

$$\dot{\sigma}_{ij}^{\Omega \setminus \mathcal{S}}(\dot{\epsilon}_{ij}) = E_{ijkl}^o \dot{\epsilon}_{kl} = E_{ijkl}^o [\dot{\hat{\epsilon}}_{kl} - \dot{\epsilon}_{kl}^{\varphi}(\llbracket \dot{u}_i \rrbracket, \llbracket \dot{u}_{i,j} \rrbracket)] \quad (17)$$

The equilibrium condition requires continuity of the traction vector (and of its rate) on \mathcal{S} , i.e., for infinitesimally close points, one over \mathcal{S} and the other in $\Omega \setminus \mathcal{S}$,

$$\dot{\sigma}_{ij}^{\Omega \setminus \mathcal{S}} n_j = \dot{\sigma}_{ij}^{\mathcal{S}} n_j \quad \text{and} \quad \sigma_{ij}^{\Omega \setminus \mathcal{S}} n_j = \sigma_{ij}^{\mathcal{S}} n_j \quad (18)$$

or, by applying Eqs. (16) and (17),

$$f_i = \left[E_{ijkl}^o [\hat{\epsilon}_{kl} - \epsilon_{kl}^{\varphi}(\llbracket u_i \rrbracket, \llbracket u_{i,j} \rrbracket)] - \sigma_{ij}^{\mathcal{S}}(\epsilon_{ij}) \right] n_j = 0 \quad (19)$$

Regularized constitutive equation

In the BEM context, the numerical solution of Eq. (19) is made by adoption of internal cells with embedded discontinuity and furnishes the displacement jump components, $\llbracket u_i \rrbracket$, required for the evaluation of ϵ_{ij}^φ . As will be clear in Sec. 5.2, these jump components are considered constants inside a cell, resulting in a null gradient tensor. Thus, for a given $\hat{\epsilon}_{ij}$ and considering Eq. (15), Eq. (19) has as only unknown variables the components $\llbracket u_i \rrbracket$, i.e., $f_i \equiv f_i(\llbracket u_i \rrbracket) = 0$.

A regularized constitutive equation, relating stress to regular strain ($\hat{\epsilon}_{ij}$), can then be defined from Eq. (17):

$$\tilde{\sigma}_{ij}(\hat{\epsilon}_{ij}) = \sigma_{ij}^{\Omega \setminus S} \left(\hat{\epsilon}_{ij} - \epsilon_{ij}^\varphi(\llbracket u_i \rrbracket)(\hat{\epsilon}_{ij}) \right) = E_{ijkl}^o (\hat{\epsilon}_{kl} - \epsilon_{kl}^\varphi) \quad (20)$$

where $\llbracket u_i \rrbracket(\hat{\epsilon}_{ij})$ represents the solution of Eq. (19).

Re-interpretation of the hardening-softening modulus in the CSDA

Another fundamental feature of the SDA is treated now in the light of the constitutive model presented in Sec. 2.1. From Eqs. (12), (1b) and (1c), it is possible to write

$$\underbrace{\sigma_{ij}^S}_{\text{bounded}} = \frac{q}{r} E_{ijkl}^o \epsilon_{kl} = \underbrace{\frac{q}{r} E_{ijkl}^o \bar{\epsilon}_{kl}}_{\text{bounded}} + \underbrace{\frac{q}{r} E_{ijkl}^o \left(\frac{1}{2h} \right) (\Delta \llbracket u_k \rrbracket n_l + \Delta \llbracket u_l \rrbracket n_k)}_{\text{unbounded when } h \rightarrow 0} \quad (21)$$

For points over S , the last term in Eq. (21) is unbounded in the strong discontinuity regime. However, even on these points, the stress components need to be bounded to maintain its physical meaning. Thus, for mathematical consistency, the following structure for the internal strain-like variable is assumed:

$$\dot{r} = \frac{1}{h} \dot{\alpha} \quad (22)$$

where $\alpha \in [0, \infty)$ is the internal strain-like variable of the associated discrete (cohesive) constitutive model, as demonstrated by Oliver (2000) and its time integration gives the required consistency to Eq. (21).

Applying now Eq. (22) to Eq. (1g), one obtains

$$\dot{q} = H \frac{1}{h} \dot{\alpha} = H^* \dot{\alpha} \quad \Rightarrow \quad H = h H^* \quad (23)$$

where H^* is called intrinsic or discrete hardening-softening modulus. Equation (23) is the mentioned re-interpretation of the continuum hardening-softening modulus, H .

3.3 Power expended in the strong discontinuity regime

Now, an explicit expression for H^* is obtained by analysing the total of energy expended in the formation of macro-cracks, \mathcal{W}_S . Firstly, with the usage of Eq. (10) and considering

negligible the energy expended during the weak discontinuity regime, the rate of the expended energy during a quasi-static deformation process in the entire domain can be written as

$$\begin{aligned}\int_{\Omega} \sigma_{ij} \dot{\epsilon}_{ij} d\Omega &= \int_{\Omega \setminus \mathcal{S}} \sigma_{ij} \dot{\epsilon}_{ij} d\Omega + \frac{1}{2} \int_{\mathcal{S}} \sigma_{ij}^{\mathcal{S}} (\llbracket \dot{u}_i \rrbracket n_j + \llbracket \dot{u}_j \rrbracket n_i) d\mathcal{S} \\ &= \int_{\Omega \setminus \mathcal{S}} \sigma_{ij} \dot{\epsilon}_{ij} d\Omega + \underbrace{\int_{\mathcal{S}} t_i^{\mathcal{S}} \llbracket \dot{u}_i \rrbracket d\mathcal{S}}_{\mathcal{P}_{\mathcal{S}}}\end{aligned}\quad (24)$$

where $t_i^{\mathcal{S}}$ is the traction vector on \mathcal{S} and $\mathcal{P}_{\mathcal{S}}$ is the power expended in the formation of the strong discontinuity. Then,

$$\mathcal{W}_{\mathcal{S}} = \int_{t_{SD}}^{t_{\infty}} \mathcal{P}_{\mathcal{S}} dt = \int_{t_{SD}}^{t_{\infty}} \int_{\mathcal{S}} t_i^{\mathcal{S}} \llbracket \dot{u}_i \rrbracket d\mathcal{S} dt = \int_{\mathcal{S}} \left[\underbrace{\int_{t_{SD}}^{t_{\infty}} t_i^{\mathcal{S}} \llbracket \dot{u}_i \rrbracket dt}_{G_f} \right] d\mathcal{S}\quad (25)$$

where t_{SD} is the time at the beginning of the strong discontinuity regime and G_f , the energy released on \mathcal{S} per unit area during the formation of a crack, is a material property, conventionally called *fracture energy*.

In Oliver (2000) it is also shown from the cohesive constitutive model, associated the continuum one of Eqs. (1), that

$$t_i^{\mathcal{S}} \llbracket \dot{u}_i \rrbracket = q \dot{\alpha}\quad (26)$$

Thus, taking the expression for the fracture energy from Eq. (25) and applying Eqs. (23) and (26),

$$G_f = \int_{t_{SD}}^{t_{\infty}} q \dot{\alpha} dt = \int_{t_{SD}}^{t_{\infty}} q \frac{\dot{q}}{H^*} dt = \int_{q_{SD}}^{q_{\infty}} q \frac{1}{H^*} dq\quad (27)$$

To obtain an exponential damage evolution law, it is necessary to define an intrinsic hardening-softening modulus of the form

$$H^* = A^* q\quad (28)$$

with A^* being a scalar constant.

Then, substituting Eq. (28) into Eq. (27), and noting that $q_{SD} = q_o = r_o = \frac{f_t}{\sqrt{E}}$ and $q_{\infty} = 0$,

$$A^* = -\frac{f_t}{G_f \sqrt{E}} \Rightarrow H^* = -\frac{f_t}{G_f \sqrt{E}} q\quad (29)$$

3.4 The variable bandwidth model

With the theoretical background presented until here, it is possible to distinguish between four steps that compose the fracture process in quasi-brittle materials, as shown in Fig. 4.

Each step is briefly described now.

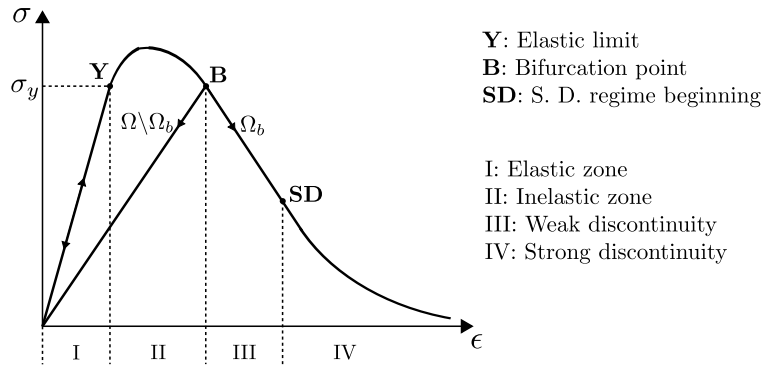


Figure 4: Quasi-brittle materials loading process.

- I. **Elastic phase:** proportional stress-strain relation until the limit point **Y**;
- II. **Inelastic phase:** non-linear behaviour with continuous strain and displacement fields;
- III. **Weak discontinuity regime:** characterized by the presence of discontinuities in the strain field. The regularized kinematic equations of Sec. 3.1 are adopted, with finite values for h , which can be interpreted as the localization bandwidth. As the loading process advances, its value reduces from h_B , on the bifurcation instant, **B**, until a null value (numerically speaking, a small parameter, k) on the point **SD**, which defines the beginning of the strong discontinuity regime;
- IV. **Strong discontinuity regime:** characterized by discontinuities in the displacement field. the regularized kinematics is also used, with $h = k \approx 0$.

The bandwidth evolution is governed by a pre-defined law. In this work, a linear variation with the stress-like internal variable of the continuous constitutive model was considered, as illustrated in Fig. 5, with $\bar{\beta} = 0.9$.

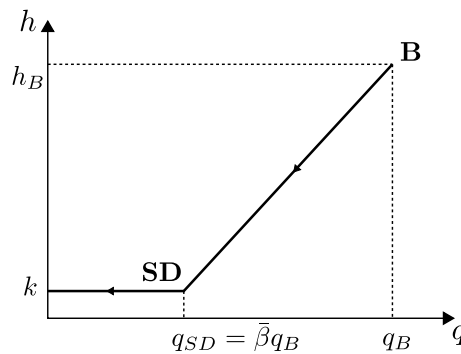


Figure 5: Bandwidth evolution law.

Particularly, the initial width of the localization band, can be obtained from Eq. (23), i.e.,

$$h_B = \left| \frac{H(q_B)}{H^*(q_B)} \right| \tag{30}$$

As detailed shown in Peixoto (2016), each phase is numerically treated by a specific damage variable evolution law, $D(r)$.

4 INTEGRAL EQUATIONS

In quasi-static mechanics of continuous media with small displacements, any point in a non-linear equilibrium path can be defined, independently of the constitutive model, as a combination of two linear parts, i.e.,

$$\dot{\epsilon}_{ij} = \dot{\epsilon}_{ij}^e + \dot{\epsilon}_{ij}^o \quad (31)$$

$$\dot{\sigma}_{ij}(\dot{\epsilon}_{ij}) = E_{ijkl}^o(\dot{\epsilon}_{kl} - \dot{\epsilon}_{kl}^o) = E_{ijkl}^o \dot{\epsilon}_{kl} - \dot{\sigma}_{ij}^o \quad (32)$$

where $\dot{\sigma}_{ij}(\dot{\epsilon}_{ij})$ is the actual stress rate.

Thus, the non-linear integral equations in the BEM context are deduced considering the existence of an initial strain field ϵ_{ij}^o , or a corresponding initial stress field $\sigma_{ij}^o = E_{ijkl}^o \epsilon_{kl}^o$. For the first option, the Somigliana's identity for displacements at internal points can be written as

$$\begin{aligned} \dot{u}_i(\boldsymbol{\xi}) = & \int_{\Gamma} u_{ij}^*(\boldsymbol{\xi}, \mathbf{X}) \dot{t}_j(\mathbf{X}) d\Gamma(\mathbf{X}) - \int_{\Gamma} t_{ij}^*(\boldsymbol{\xi}, \mathbf{X}) \dot{u}_j(\mathbf{X}) d\Gamma(\mathbf{X}) \\ & + \int_{\Omega} u_{ij}^*(\boldsymbol{\xi}, \mathbf{X}) \dot{b}_j(\mathbf{X}) d\Omega(\mathbf{X}) + \int_{\Omega} \sigma_{ijk}^*(\boldsymbol{\xi}, \mathbf{X}) \dot{\epsilon}_{jk}^o(\mathbf{X}) d\Omega(\mathbf{X}) \end{aligned} \quad (33)$$

where u_j and t_j represents the displacement and the traction fields at the boundary Γ and b_j are body forces in the domain Ω . The terms u_{ij}^* , t_{ij}^* and σ_{ijk}^* are Kelvin's fundamental solutions, representing respectively, at a field point \mathbf{X} , displacements and tractions in direction j and stress components jk due to a unit concentrated force applied at the collocation point $\boldsymbol{\xi}$ acting in direction i . Here, the collocation point is assumed to be internal, i.e., $\{\boldsymbol{\xi} \in \Omega \text{ and } \boldsymbol{\xi} \notin \Gamma\}$. Expressions for these fundamental solutions are presented in many literature texts, such as Telles (1983), Gao and Davies (2002) and Aliabadi (2002).

If the collocation point is located in domain's boundary, the fundamental solutions' second-order tensors introduce a weakly and a strongly singular character, respectively for the first and second integrals in Eq. (33). Thus, the correct evaluation of the boundary displacement integral equation requires, in this case, a limit process considering a radius of exclusion around the singular point, leading to the following expression:

$$\begin{aligned} c_{ij}(\boldsymbol{\xi}) \dot{u}_j(\boldsymbol{\xi}) = & \int_{\Gamma} u_{ij}^*(\boldsymbol{\xi}, \mathbf{X}) \dot{t}_j(\mathbf{X}) d\Gamma(\mathbf{X}) - \int_{\Gamma} t_{ij}^*(\boldsymbol{\xi}, \mathbf{X}) \dot{u}_j(\mathbf{X}) d\Gamma(\mathbf{X}) \\ & + \int_{\Omega} u_{ij}^*(\boldsymbol{\xi}, \mathbf{X}) \dot{b}_j(\mathbf{X}) d\Omega(\mathbf{X}) + \int_{\Omega} \sigma_{ijk}^*(\boldsymbol{\xi}, \mathbf{X}) \dot{\epsilon}_{jk}^o(\mathbf{X}) d\Omega(\mathbf{X}) \end{aligned} \quad (34)$$

where $c_{ij}(\boldsymbol{\xi})$ is a function of the boundary's geometry around the collocation point and the elastic properties of the material. It is also important to emphasize that the second integral exists only in the Cauchy's Principal Value (CPV) sense, as indicated by the crossed integral symbol.

Furthermore, internal strains can be obtained by taking the symmetric part of the gradient

of Eq. (33), related to the collocation point, resulting in

$$\begin{aligned} \dot{\epsilon}_{ij}(\boldsymbol{\xi}) = & \int_{\Gamma} u_{ijk}^*(\boldsymbol{\xi}, \mathbf{X}) \dot{t}_k(\mathbf{X}) d\Gamma(\mathbf{X}) - \int_{\Gamma} t_{ijk}^*(\boldsymbol{\xi}, \mathbf{X}) \dot{u}_k(\mathbf{X}) d\Gamma(\mathbf{X}) \\ & + \int_{\Omega} u_{ijk}^*(\boldsymbol{\xi}, \mathbf{X}) \dot{b}_k(\mathbf{X}) d\Gamma(\mathbf{X}) + \int_{\Omega} \sigma_{ijkl}^*(\boldsymbol{\xi}, \mathbf{X}) \dot{\epsilon}_{kl}^o(\mathbf{X}) d\Omega(\mathbf{X}) + F_{ijkl}^{ee} \dot{\epsilon}_{kl}^o(\boldsymbol{\xi}) \end{aligned} \quad (35)$$

where the last domain integral have a strongly singular kernel when the collocation and field points coincide and, again, its evaluation exists only in the CPV sense. Tensors u_{ijk}^* , t_{ijk}^* and σ_{ijkl}^* are respectively obtained by taking the gradients of fundamental solutions u_{ij}^* , t_{ij}^* and σ_{ijk}^* , while F_{ijkl}^{ee} is the free term, which existence was firstly verified by Bui (1978).

The above integral equations were obtained considering continuous fields. However, from the similarities between Eqs. (32) and (20), integral equations concerning discontinuity surfaces in the domain can be obtained, resulting in expressions of the same forms, considering only the substitution of terms depicted in Table 1. A more formal demonstration can be found in Manzoli and Venturini (2004) and Peixoto (2016).

Table 1: Correspondent terms for integral equations

Standard Integral Equations	IE with discontinuity surface
u_i	\hat{u}_i
ϵ_{ij}	$\hat{\epsilon}_{ij}$
ϵ_{ij}^o	ϵ_{ij}^φ

5 NUMERICAL ASPECTS

From the division of the problem's boundary in elements and part of the domain (with non-zero initial fields) in cells, as usual in the BEM, the application of the integral equations of Sec. 4 results in a set of matrix equations, which can be reorganized, producing a non-linear equation in terms of the total strains. Such procedure was named as implicit formulation (Telles and Carrer, 1991) and was adopted in present work. A complete solution strategy can be seen in Peixoto (2016).

Additional numerical aspects regarding internal cells with embedded discontinuity, evaluation of displacement jumps, the regularized constitutive model tangent operator and the algorithm to track the discontinuity line, which includes automatic cells generation, are presented in the following.

5.1 Cells with embedded discontinuity

From conditions of Eq. (13), weak and strong discontinuity dissipative effects are restricted to the sub-domain Ω_φ , defined in Fig. 3b, and only this region needs to be discretized by cells with embedded discontinuity. Moreover, regions under inelastic behaviour, however in a pre-bifurcation phase, also need to be divided by (standard) cells, as illustrated in Fig. 6a.

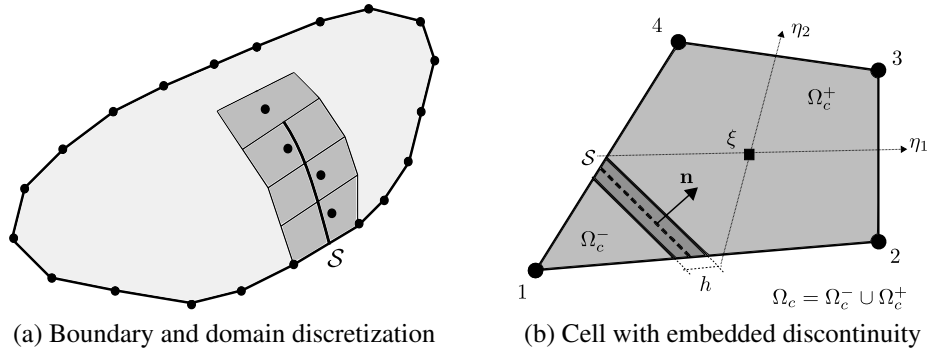


Figure 6: BEM discretization of a solid with discontinuity surface

For each internal cell with embedded discontinuity, typically represented in Fig. 6b, only one collocation point is adopted and the field ϵ_{ij}^φ is considered constant inside the entire cell domain, i.e., for $\mathbf{X} \in \Omega_c$,

$$\left\{ \epsilon_{11}^\varphi(\mathbf{X}) \quad \epsilon_{22}^\varphi(\mathbf{X}) \quad \epsilon_{12}^\varphi(\mathbf{X}) \right\}^T \approx \left\{ \epsilon_{11}^{\varphi,c} \quad \epsilon_{22}^{\varphi,c} \quad \epsilon_{12}^{\varphi,c} \right\}^T = \{\epsilon^{\varphi,c}\} \quad (36)$$

However, the geometry of each cell is parametrized by conventional linear shape functions defined by natural coordinates η_i , i.e.,

$$X_j(\eta_1, \eta_2) \approx M^\alpha(\eta_1, \eta_2) X_j^\alpha \quad (37)$$

where index α refer to corner points (numbered from 1 to 4 in Fig. 6b).

Thus, in a cell with embedded discontinuity, one can distinguish an internal collocation point and a set of geometry interpolation points. Other important attribute is the orientation of the discontinuity line (given by its normal vector).

The geometry interpolation functions can also be used to define the function $\varphi(\mathbf{X})$ inside the cell, since the conditions of Eq. (13) are fulfilled by the choice:

$$\varphi(\mathbf{X}(\eta_1, \eta_2)) = \sum_{\alpha^+} M^{\alpha^+}(\eta_1, \eta_2) \quad (38)$$

where the summation is taken over the interpolation functions associated to the geometric corners located at Ω_c^+ side of the cell. For example, in Fig. 6b, $\alpha^+ = 2, 3, 4$.

5.2 Evaluation of displacement jumps

The displacement jump inside a cell with embedded discontinuity is obtained from the numerical solution of Eq. (19), i.e., the interface equilibrium equation. To do this, the functions $\llbracket u_i \rrbracket(\mathbf{X})$ are also considered as constants inside the cell domain, i.e.,

$$\begin{cases} \llbracket u_i \rrbracket(\mathbf{X}) \approx \left\{ \llbracket u_1^c \rrbracket \quad \llbracket u_2^c \rrbracket \right\}^T = \{\llbracket u^c \rrbracket\} & \text{for } \mathbf{X} \in \Omega_c \\ \llbracket u_{i,j} \rrbracket(\mathbf{X}) = 0 & \text{for } \mathbf{X} \in \Omega_c \end{cases} \quad (39)$$

Using Eqs. (15) and (39), the vector of Eq. (36) can be written in terms of the displacement jump:

$$\{\epsilon^{\varphi,c}\} = \begin{bmatrix} \varphi_{,1} & 0 \\ 0 & \varphi_{,2} \\ \frac{1}{2}\varphi_{,2} & \frac{1}{2}\varphi_{,1} \end{bmatrix} \begin{Bmatrix} \llbracket u_1 \rrbracket \\ \llbracket u_2 \rrbracket \end{Bmatrix} = [\nabla\varphi]\{\llbracket u \rrbracket\} \quad (40)$$

where, from Eqs. (37) and (38),

$$\varphi_{,i} = \frac{\partial\varphi}{\partial\eta_k} \frac{\partial\eta_k}{\partial X_i} = \left(\frac{\partial M^\alpha}{\partial\eta_k} X_i^\alpha \right)^{-1} \left(\frac{\partial}{\partial\eta_k} \left[\sum_{\alpha^+} M^{\alpha^+} \right] \right) \quad (41)$$

Thus, using Eqs. (39) and (40), the following matrix form of Eq. (19) is obtained:

$$[\bar{N}^c]^T \left([E^o]\{\hat{\epsilon}^c\} - [E^o][\nabla\varphi]\{\llbracket u \rrbracket\} - \{\sigma^S(\{\hat{\epsilon}^c\} - [\nabla\varphi]\{\llbracket u \rrbracket\} + \frac{1}{h}[N^c]\{\llbracket u \rrbracket\})\} \right) = \{0\} \quad (42)$$

where,

$$[\bar{N}^c] = \begin{bmatrix} n_1 & 0 & n_2 \\ 0 & n_2 & n_1 \end{bmatrix}^T; \quad [N^c] = \begin{bmatrix} n_1 & 0 & \frac{1}{2}n_2 \\ 0 & n_2 & \frac{1}{2}n_1 \end{bmatrix}^T \quad (43)$$

Finally, Eq. (42) is solved by Newton's iterative method, noting that its linearised form, for a known $\{\hat{\epsilon}^c\}$, is given by

$$\{f\}_{j-1} + \left[\frac{\partial\{f\}}{\partial\{\llbracket u \rrbracket\}} \right]_{j-1} \{\delta\llbracket u \rrbracket\}_j \approx \{0\} \quad (44)$$

where j is an iterative index and

$$\left[\frac{\partial\{f\}}{\partial\{\llbracket u \rrbracket\}} \right]_{j-1} = [\bar{N}^c]^T \left[- [E^o][\nabla\varphi] - \left[\frac{\partial\sigma^S}{\partial\epsilon} \right]_{j-1} \left[\frac{1}{h}[N^c] - [\nabla\varphi] \right] \right] \quad (45)$$

In Eq. (45), the term $\left[\frac{\partial\sigma^S}{\partial\epsilon} \right]$ is the tangent operator of the continuum constitutive model used to represent the dissipative effects over the discontinuity line \mathcal{S} - in this case, Eq. (3).

5.3 Regularized constitutive equation

The matrix form of Eq. (20), for an internal cell, is given by

$$\{\tilde{\sigma}(\hat{\epsilon}^c)\} = [E^o](\{\hat{\epsilon}^c\} - [\nabla\varphi]\{\llbracket u \rrbracket\}) = [E^o](\{\hat{\epsilon}^c\} - \{\epsilon^{\varphi,c}\}) \quad (46)$$

Thus, the tangent operator associated to this regularized constitutive equation and necessary for the solution of implicit BEM formulation's, can be obtained from Eq. (46), i.e.,

$$\left[\frac{\partial\tilde{\sigma}}{\partial\hat{\epsilon}^c} \right] = [E^o] \left([I] - [\nabla\varphi] \left[\frac{\partial\{f\}}{\partial\{\llbracket u \rrbracket\}} \right]^{-1} [\bar{N}^c]^T \left([E^o] - \left[\frac{\partial\sigma^S}{\partial\epsilon} \right] \right) \right) \quad (47)$$

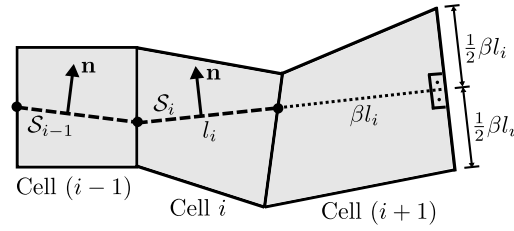


Figure 7: Discontinuity line tracking schema

5.4 Discontinuity line tracking algorithm

To track the discontinuity line across the solid domain, an algorithm that automatically generates cells was implemented, as illustrated in Fig. 7.

A cell under elastic regime or with damage in continuous media (before bifurcation) always exists at the front of the last point of the discontinuity line. When the bifurcation condition is satisfied in this cell, a straight discontinuity segment is introduced (e.g., S_i in Cell i) in a orientation defined by the bifurcation analysis. Continuity of the discontinuity line is imposed, as shown for segments S_{i-1} and S_i , in the common edge of adjacent cells. A new cell (Cell $(i + 1)$ in Fig. 7) is then created following the next steps:

- i. The edge of the previous cell that contains the current final point of the discontinuity line is taken as a first edge of the new cell;
- ii. A straight line segment is drawn from the front of the discontinuity segment of the previous cell, in its same orientation and with its length weighted by a factor β (a pre-defined scalar constant);
- iii. A second edge of the new cell is created perpendicularly to this line segment, with its same size and taking its final point as the central edge's point;
- iv. The other two edges are created by connecting the endpoints of these two edges.

Numerically speaking, the introduction of a new cell means increases of specific matrices, which can be done in any iteration of the incremental-iterative solution strategy.

6 NUMERICAL EXAMPLES

To demonstrate the efficiency of the above methodology in the simulation of quasi-brittle materials, two numerical examples of mixed-mode concrete fracture are presented.

6.1 Example 1: Arrea and Ingraffea (1982)

In this first example, the four point bending of a notched plain concrete beam, experimentally analysed by Arrea and Ingraffea (1982), is addressed. The geometry, loads, boundary conditions and material properties are presented in Fig. 8.

The vertical displacement of point A was used to control the non-linear analysis progression. The problem's boundary was divided in 642 linear elements and an initial square cell with diagonal of 1.6 mm was introduced in the tip of the initial notch. A value of $\beta = 1.001$ was adopted in the tracking algorithm. The final mesh is presented in Fig. 9.

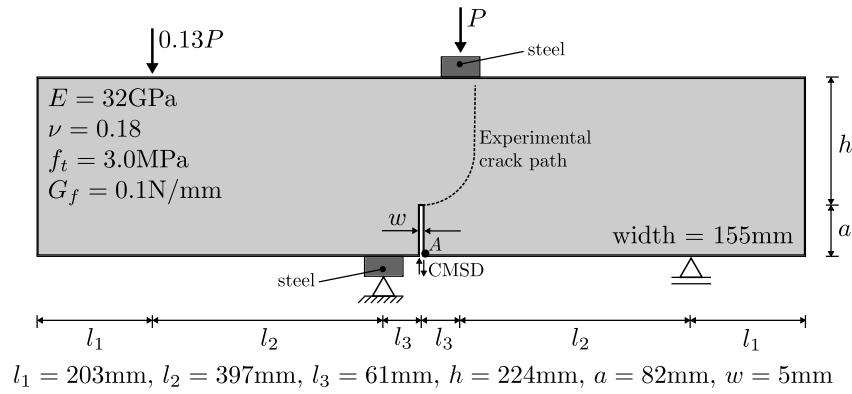


Figure 8: Example 1 - Four point bending (Arrea and Ingraffea, 1982)

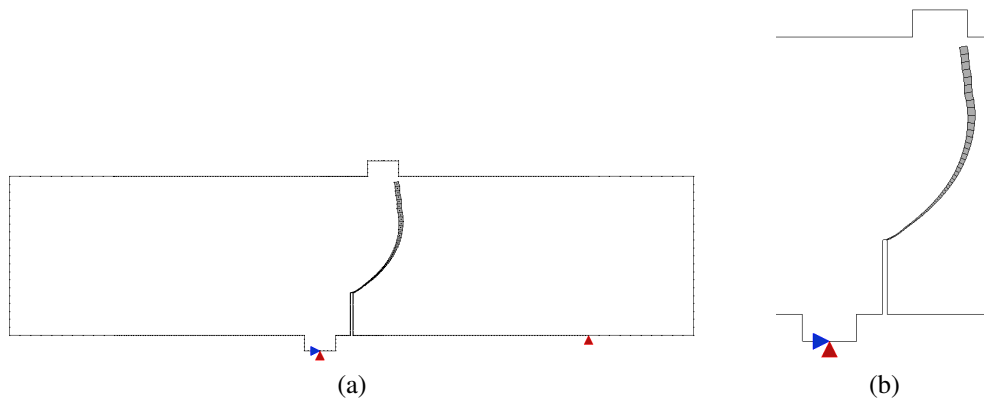


Figure 9: Example 1 - (a) Complete final mesh, (b) detail

The curve of load P versus the Crack Mouth Sliding Displacement (CMSD) of the original notch is presented in Fig. 10. The numerical results are plotted over the empirical envelopment and a good accuracy can be observed.

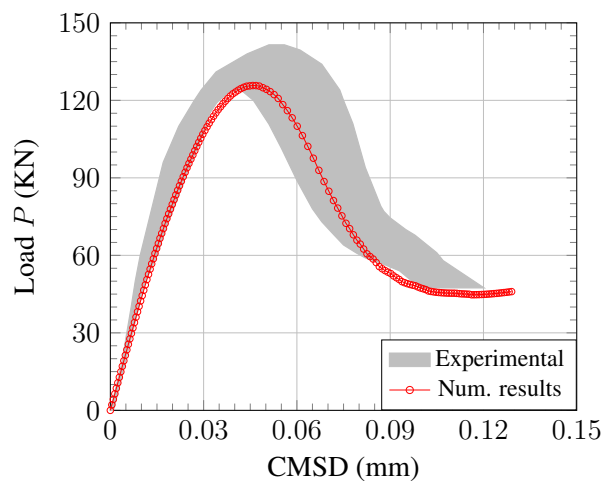


Figure 10: Example 1 - Results for load P vs. CMSD (Crack Mouth Sliding Displacement)

6.2 Example 2: Gálvez et al. (1998)

Now, one of the four point bending of a notched plain concrete beam, experimentally studied by Gálvez et al. (1998), is analysed. The geometry, loads, boundary conditions and material properties are presented in Fig. 11.

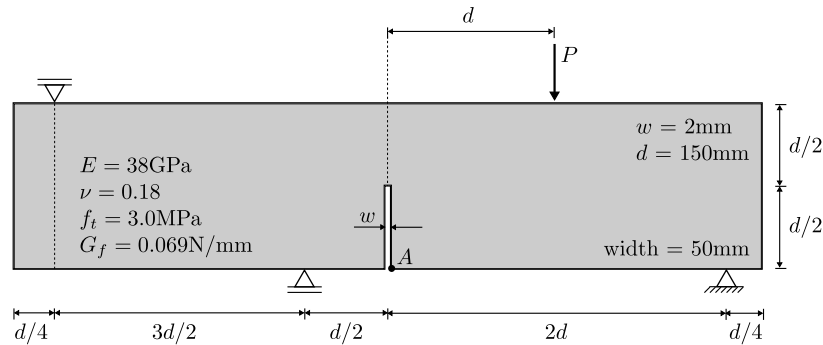


Figure 11: Example 2 - Four point bending (Gálvez et al., 1998)

The vertical displacement of point *A* was used to control the non-linear analysis progression. The problem's boundary was divided in 607 linear elements and an initial square cell with diagonal of 0.6 mm was introduced in the tip of the initial notch. Again, a value of $\beta = 1.001$ was adopted in the tracking algorithm. The final mesh is presented in Fig. 12.

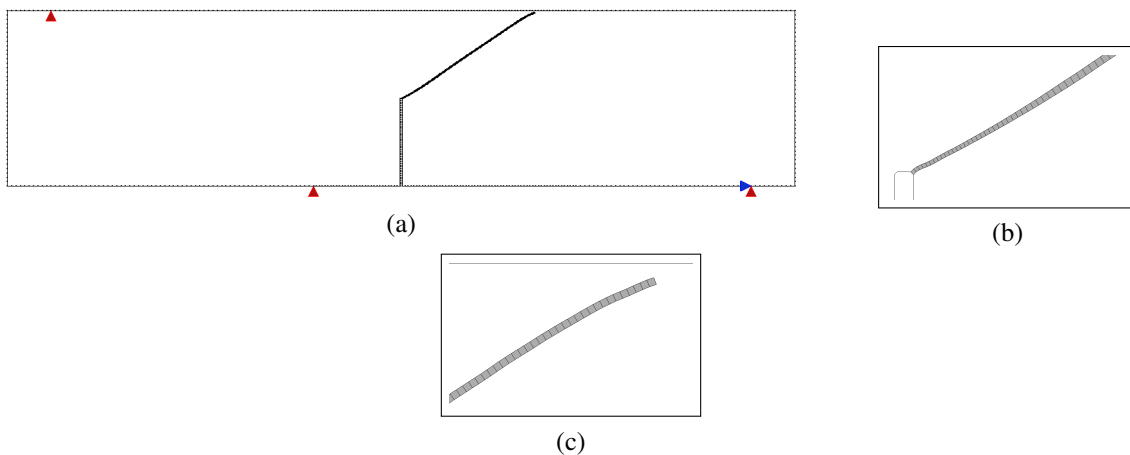


Figure 12: Example 2 - (a) Complete final mesh, (b) initial cells detail, (c) final cells detail

The curve of load *P* versus the vertical displacement of the loaded point is presented in Fig. 13. Again, the numerical results are plotted over the empirical envelopment and a good accuracy can be observed.

7 CONCLUDING REMARKS

Two dimensional concrete fracture problems were addressed using the CSDA with the BEM. An isotropic damage constitutive model was adopted to represent the material behaviour before and after the bifurcation time, characterized by the singularity of the localization tensor. When the strong discontinuity conditions are not achieved at this time, a weak discontinuity

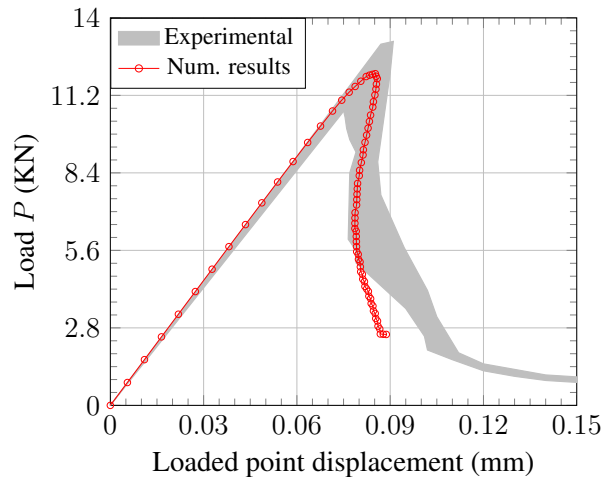


Figure 13: Example 2 - Results for load P vs. displacement of the loaded point

regime is imposed with a pre-defined bandwidth variation law, precluding the strong one. Both regimes are treated with the same set of kinematic equations, which contains a scale bandwidth factor, h . In that way, weak and strong discontinuities regimes are indiscriminately represented by a single discontinuity line, which is embedded into internal cells.

To track the crack path, an automatic cells generation algorithm was implemented. The onset of a discontinuity segment is permitted to occur even during the iterative process of a load step, and not only after its convergence. With this procedure, the analysis become less sensitive to load steps sizes and simple control methods can be employed. However, it seems to be indispensable the complete bifurcation analysis, with a continuum dissipation stage precluding the discontinuity inception, for a correct crack trajectory prediction.

Finally, very good agreement of the numerical analysis were verified when compared to experimental data available in the literature.

ACKNOWLEDGEMENTS

The authors gratefully acknowledge the important support of the Brazilian research agencies FAPEMIG (in Portuguese “Fundação de Amparo à Pesquisa do Estado de Minas Gerais”), CNPq (in Portuguese “Conselho Nacional de Desenvolvimento Científico e Tecnológico”).

REFERENCES

- Aliabadi, M. H., 2002. *The boundary element method: volume 2 - applications in solids and structures*. John Wiley & Sons, Chichester.
- Arrea, M. & Ingraffea, A. R., 1982. Mixed-mode crack propagation in mortar and concrete. Technical report, 81-13, Department of Structural Engineering, Cornell University, Ithaca, USA.
- Benallal, A., Botta, A. S., & Venturini, W. S., 2006. On the description of localization and failure phenomena by the boundary element method. *Computer Methods in Applied Mechanics and Engineering*, vol. 195, pp. 5833–5856.

- Benallal, A., Fudoli, C. A., & Venturini, W. S., 2002. An implicit BEM formulation for gradient plasticity and localization phenomena. *International Journal for Numerical Methods in Engineering*, vol. 53, pp. 1853–1869.
- Botta, A. S., Venturini, W. S., & Benallal, A., 2005. BEM applied to damage models emphasizing localization and associated regularization techniques. *Engineering Analysis with Boundary Elements*, vol. 29, pp. 814–827.
- Bui, H. D., 1978. Some remarks about the formulation of three-dimensional thermoelastoplastic problems by integral equations. *International Journal of Solids and Structures*, vol. 14, pp. 935–939.
- Gálvez, J. C., Elices, M., Guinea, G. V., & Planas, J., 1998. Mixed mode fracture of concrete under proportional and nonproportional loading. *International Journal of Fracture*, vol. 94, pp. 267–284.
- Gao, X.-W. & Davies, T. G., 2002. *Boundary Element Programming in Mechanics*. Cambridge University Press, Cambridge.
- García, R., Flórez-López, J., & Cerrolaza, M., 1999. A boundary element formulation for a class of non-local damage models. *International Journal of Solids and Structures*, vol. 36, pp. 3617–3638.
- Herding, U. & Kuhn, G., 1996. A field boundary element formulation for damage mechanics. *Engineering Analysis with Boundary Elements*, vol. 18, pp. 137–147.
- Lin, F.-B., Yan, G., Bažant, Z. P., & Ding, F., 2002. Non-local strain softening model of quasi-brittle materials using boundary element method. *Engineering Analysis with Boundary Elements*, vol. 26, pp. 417–424.
- Manzoli, O. L., Pedrini, R. A., & Venturini, W. S., 2009. Strong discontinuity analysis in solid mechanics using boundary element method. In Spoutzakis, E. J. & Aliabadi, M. H., eds, *Avances in Boundary Element Techniques X*, pp. 323–329, Atenas, Grcia.
- Manzoli, O. L. & Venturini, W. S., 2004. Uma formulao do MEC para simulao numrica de descontinuidades fortes. *Revista Internacional de Mtodos Numricos para Clculo y Diseo en Ingeniera*, vol. 20, n. 3, pp. 215–234.
- Manzoli, O. L. & Venturini, W. S., 2007. An implicit BEM formulation to model strong discontinuities. *Computational Mechanics*, vol. 40, pp. 901–909.
- Mendelson, A., 1973. Boundary integral methods in elasticity and plasticity. Technical report, NASA TN D-7418, USA.
- Mukherjee, S., 1977. Corrected boundary-integral equations in planar thermoelastoplasticity. *International Journal of Solids and Structures*, vol. 13, pp. 331–335.
- Oliver, J., 1996. Modelling strong discontinuities in solid mechanics via strain softening constitutive equations. Part 1: Fundamentals. *International Journal for Numerical Methods in Engineering*, vol. 39, pp. 3575–3600.
- Oliver, J., 2000. On the discrete constitutive models induced by strong discontinuity kinematics

and continuum constitutive equations. *International Journal of Solids and Structures*, vol. 37, pp. 7207–7229.

Oliver, J., Huespe, A. E., Blanco, S., & Linero, D. L., 2006. Stability and robustness issues in numerical modeling of material failure with the strong discontinuity approach. *Computer Methods in Applied Mechanics and Engineering*, vol. 195, pp. 7093–7114.

Peixoto, R. G., 2016. *Análise de degradação material, bifurcação e transição entre descon-tinuidades fracas e fortes através do método dos elementos de contorno*. PhD thesis, Universidade Federal de Minas Gerais, Belo Horizonte.

Peixoto, R. G., Ribeiro, G. O., Pitangueira, R. L. S., & Penna, S. S., 2015. Strain localization in the boundary element method: the strong discontinuity approach as a limit case. In Dumont, N. A., ed, *Proceedings of the XXXVI Iberian Latin-American Congress on Computational Meth-ods in Engineering - CILAMCE*, Rio de Janeiro, RJ, Brazil.

Rajgelj, S., Amadio, C., & Nappi, A., 1992. Application of damage mechanics concepts to the boundary element method. In Brebbia, C. A. & Ingber, M. S., eds, *Seventh International Conference on Boundary Element Technology*, pp. 617–634.

Riccardella, P. C., 1973. An implementation of the boundary integral technique for planar prob-lems in elasticity and elastoplasticity. Technical report, SM-73-10, Carnegie Mellon University, Pittsburgh, USA.

Rice, J. R. & Rudnicki, J. W., 1980. A note on some features of the theory of localization of deformation. *International Journal of Solids and Structures*, vol. 16, pp. 597–605.

Simo, J. C., Oliver, J., & Armero, F., 1993. An analysis of strong discontinuities induced by strain-softening in rate-independent inelastic solids. *Computational Mechanics*, vol. 12, pp. 277–296.

Sládek, J., Sládek, V., & Bažant, Z. P., 2003. Non-local boundary integral formulation for softening damage. *International Journal for Numerical Methods in Engineering*, vol. 57, pp. 103–116.

Swedlow, J. L. & Cruse, T. A., 1971. Formulation of boundary integral equations for three dimensional elastoplastic flow. *Journal of Solids and Structures*, vol. 7, pp. 1673–1683.

Telles, J. C. F., 1983. *Boundary Element Method applied to inelastic problems*. Springer-Verlag, Berlin.

Telles, J. C. F. & Brebbia, C. A., 1979. On the application of the boundary element method to plasticity. *Applied Mathematical Modelling*, vol. 3, n. 4, pp. 466–470.

Telles, J. C. F. & Carrer, J. A. M., 1991. Implicit procedures for the solution of elastoplastic problems by the boundary element method. *Mathematical and Computer Modelling*, vol. 15, pp. 303–311.

van der Giessen, E. & de Borst, R., 1998. Introduction to material instabilities in solids. In de Borst, R. & van der Giessen, E., eds, *Material instabilities in solids*, chapter 1. John Wiley & Sons, Chichester.